N-Phenylacetanoyl-L-Homoserine Lactones Can Strongly Antagonize or Super-Agonize Quorum Sensing in *Vibrio fischeri*

Grant D. Geske, Jennifer C. O'Neill, and Helen E. Blackwell*

Department of Chemistry, University of Wisconsin – Madison, 1101 University Avenue, Madison, WI 53706-1322

E-mail: blackwell@chem.wisc.edu

Supporting Information.

* To whom correspondence should be addressed.

General experimental information.

General. ^{1}H NMR spectra were recorded on a Bruker AC-300 spectrometer in deuterated solvents at 300 MHz. Electrospray ionization (ESI) MS were obtained using a Shimadzu LCMS-2010a system (Columbia, MD) equipped with two pumps (LC-10ADvp), controller (SCL-10Avp), UV diode array detector (SPD-M10Avp), and single quadrupole analyzer. GC-MS data were obtained using a Shimadzu GC-17A system (Columbia, MD) equipped with a QP-5000 mass spectrometer. A Restek RTX-5 cross bond 95% polysiloxane GC column was used with following general gradient: injection temperature 300 °C; initial oven temperature 100 °C; hold 3 min; ramp at 20 °C/min to 300 °C; hold 2–15 min for a total run time of 15–30 min.

All chemical reagents were purchased from commercial sources (Alfa-Aesar, Aldrich, Acros, and Sigma) and used without further purification. Solvents were purchased from commercial sources (Aldrich and J.T. Baker) and used as is, with the exception of dichloromethane (CH_2Cl_2), which was distilled over calcium hydride immediately prior to use. All solid-phase syntheses were performed using aminomethyl polystyrene resin (NovaBiochem, 100–200 mesh; loading 1.1–1.2 mmol/g).

Microwave instrumentation. Microwave-assisted solid-phase reactions were carried out using either a Milestone Microsynth Labstation[1] or CEM Discover[2] commercial microwave (MW) reactor. All MW-assisted reactions were performed using temperature control to monitor MW irradiation.

Solid-phase library synthesis techniques. Solid-phase reactions were performed in either 100 mL round bottom flasks in the Milestone MW reactor or 10 mL glass CEM MW vessels (part # 908035) in the CEM MW reactor. Liquid reagents were dispensed during synthesis using either disposable syringes or Brinkman Eppendorf pipettmen (calibrated for variable solvent delivery) equipped with disposable polypropylene pipette tips. Between synthesis steps, the solid-phase resin was washed with solvents stored in polypropylene Nalgene squirt bottles. Large quantities of resin were washed in a standard glass frit. Small quantities of resin were washed on a Vac-Man vacuum manifold (Promega, part #: A7231) in 8 mL polypropylene sample reservoirs (Alltech, part #: 210208) equipped with 20 μm frits (Alltech, part #: 211408).

Structures of 24-member PHL library 11.

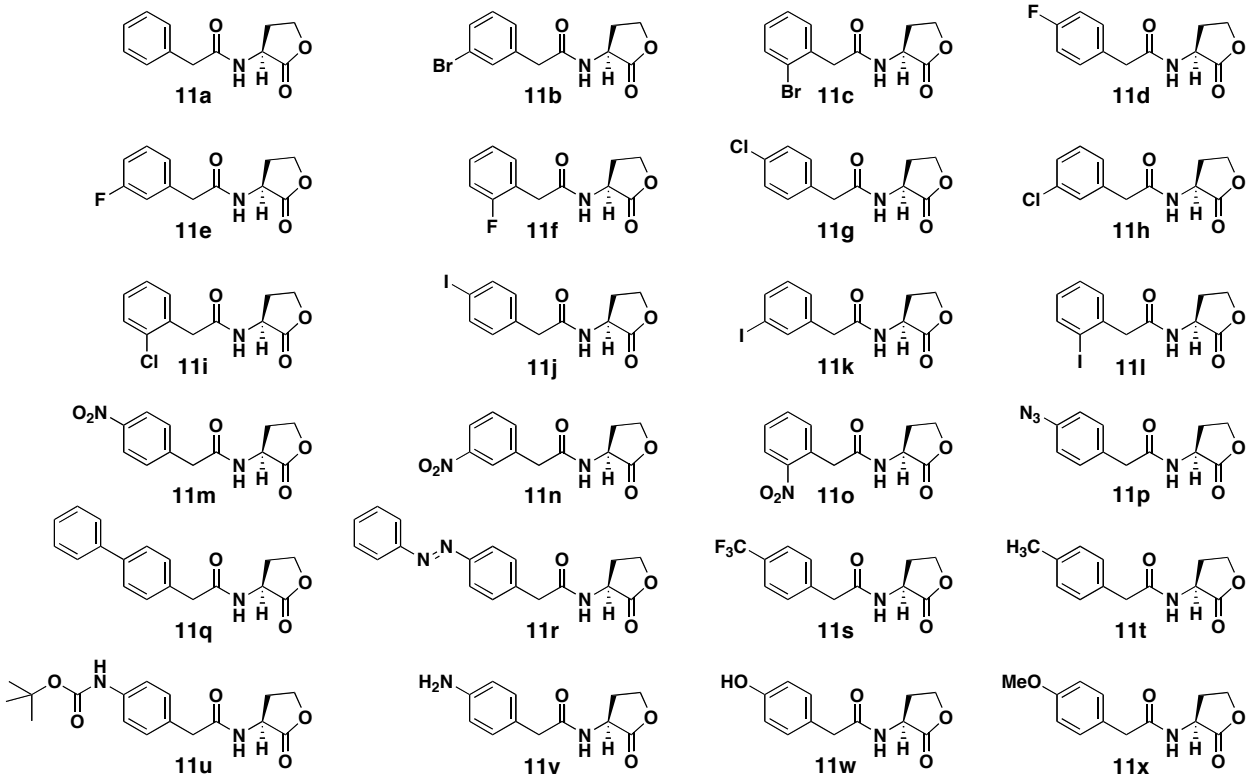

Characterization data for AHL derivatives.

Characterization data for OHHL (**1**) and control compounds **2**, **3**, and **5** matched those published previously.[3] ^{1}H NMR, ^{13}C NMR, IR, MS, and optical rotation data was as expected for control compound **4** and PHL library **11**. GC-MS (or ^{1}H NMR and MS for **11u**) data is provided in Table S-1 as proof of purity and identity for these compounds.

Table S-1. Purity and Mass Data of AHL Derivatives.

Compound Expected mol. wt. Purity	Structure	GC-MS data
DMSO blank		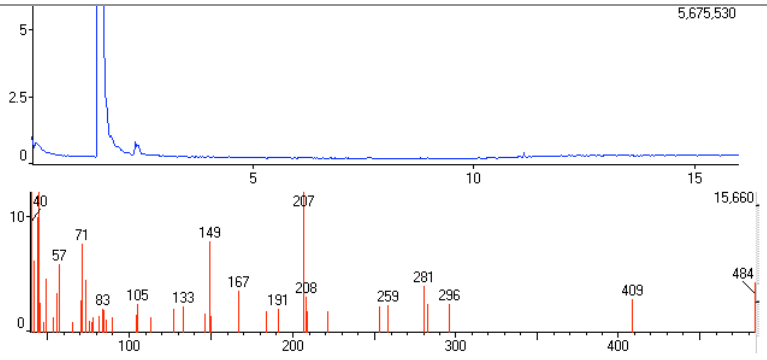
4[a] 235.3 97.6%	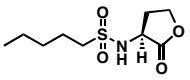	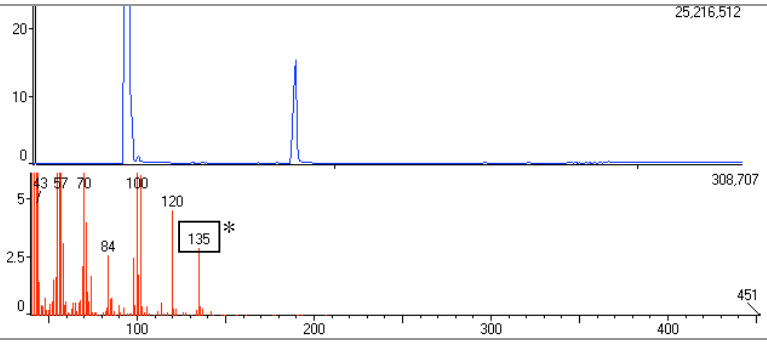
11a 219.2 >99%	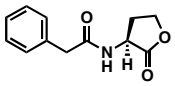	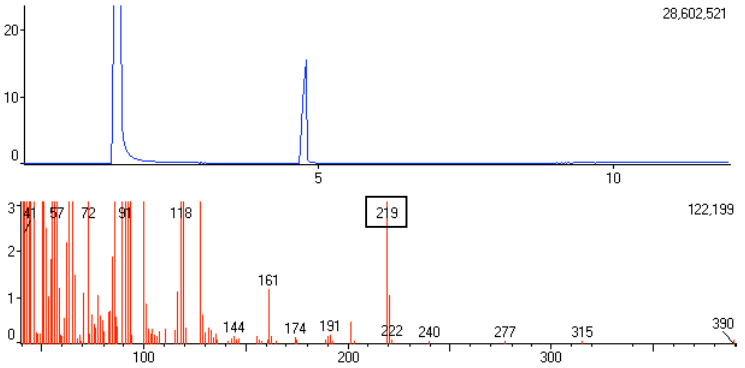
11b 298.1 >99%	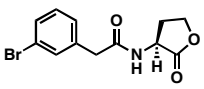	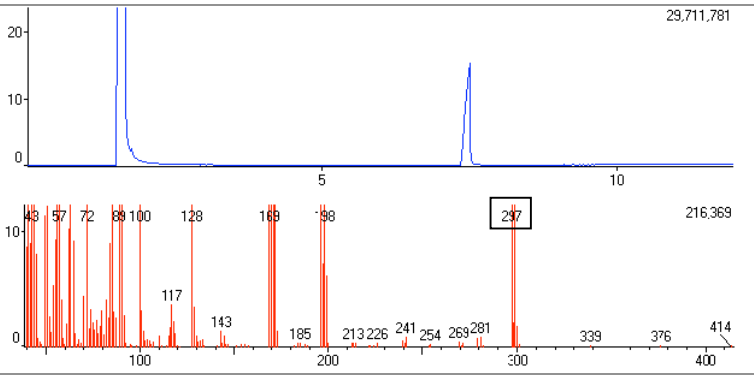

11c[b] 298.1 >99%	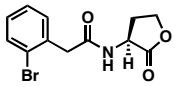	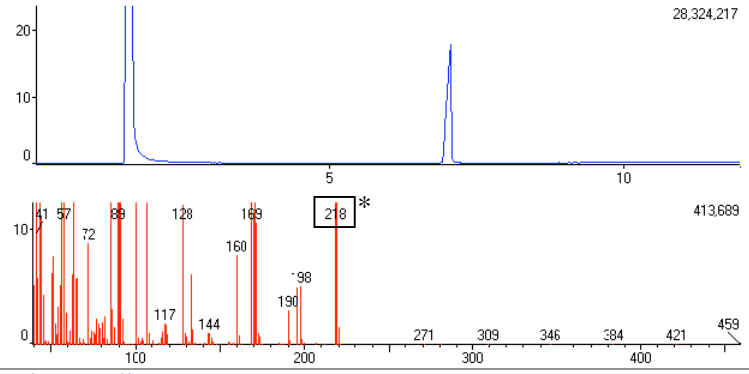
11d 237.2 >99%	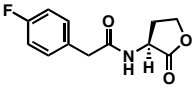	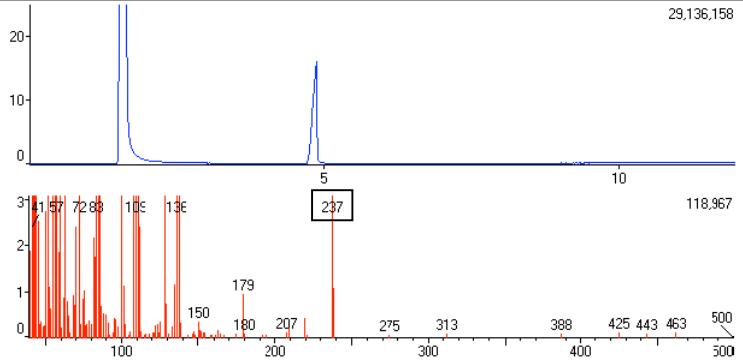
11e 237.2 >99%	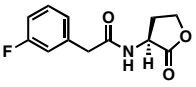	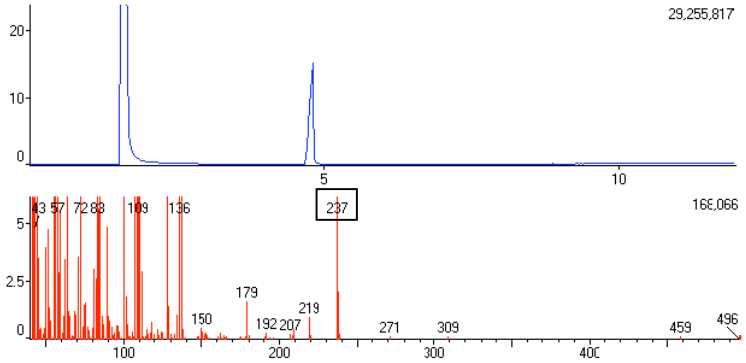
11f 237.2 >99%	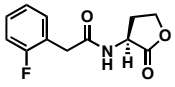	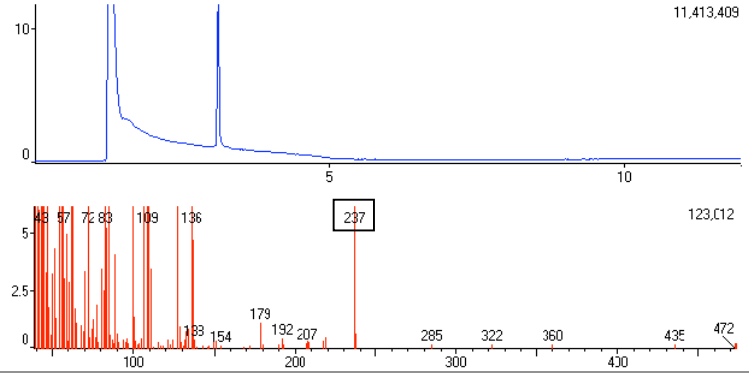

11g 253.7 >99%	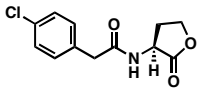	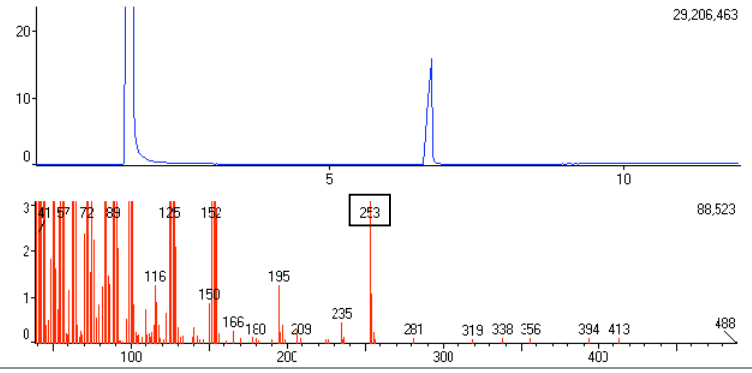
11h 253.7 >99%	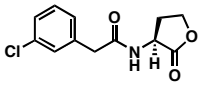	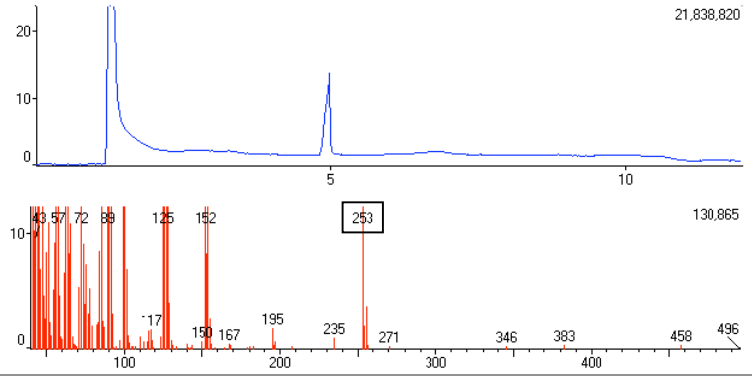
11i[b] 253.7 >99%	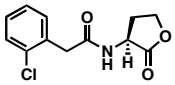	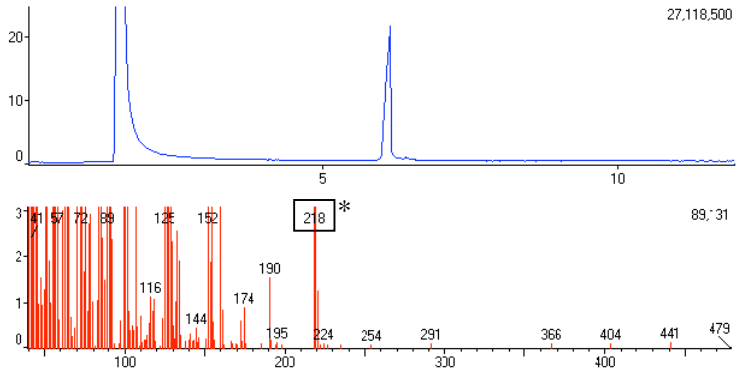
11j 345.1 >99%	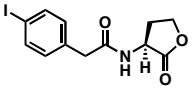	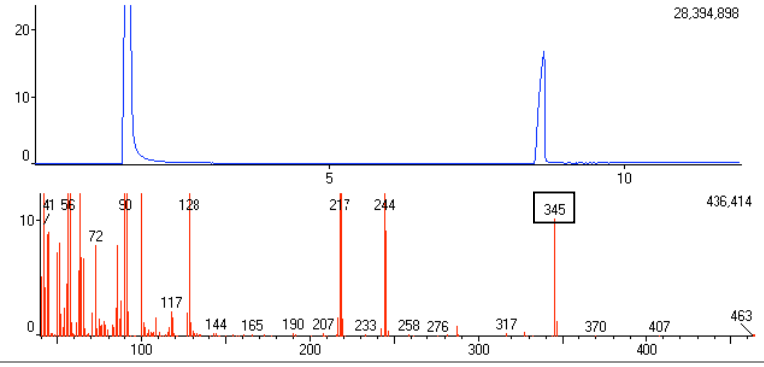

11k 345.1 96.9%	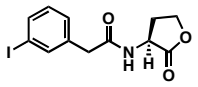	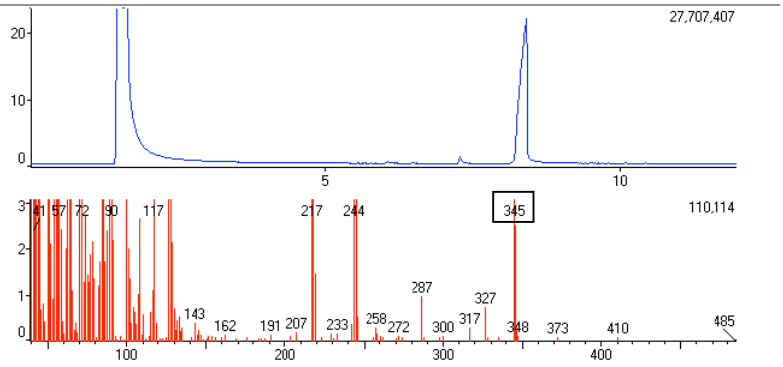
11l[a,b] 345.1 98.3%	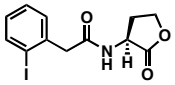	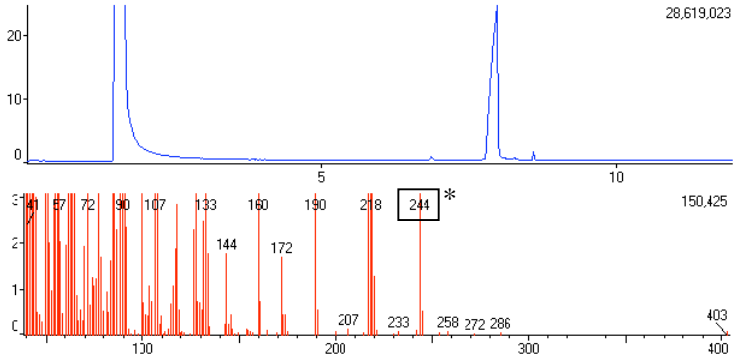
11m 264.2 >99%	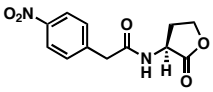	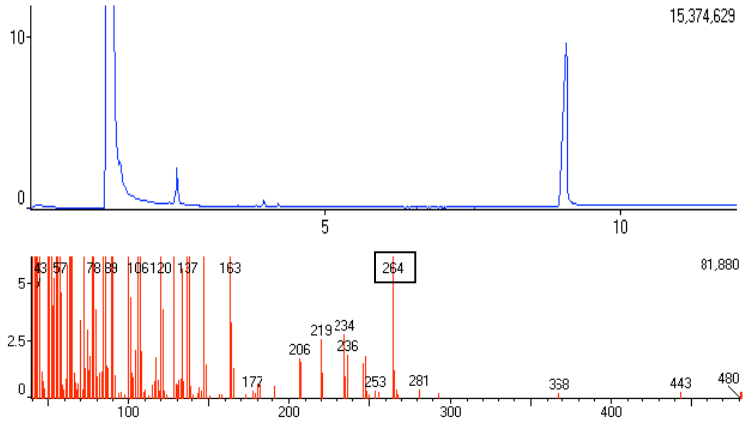
11n 264.2 97.5%	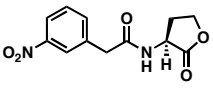	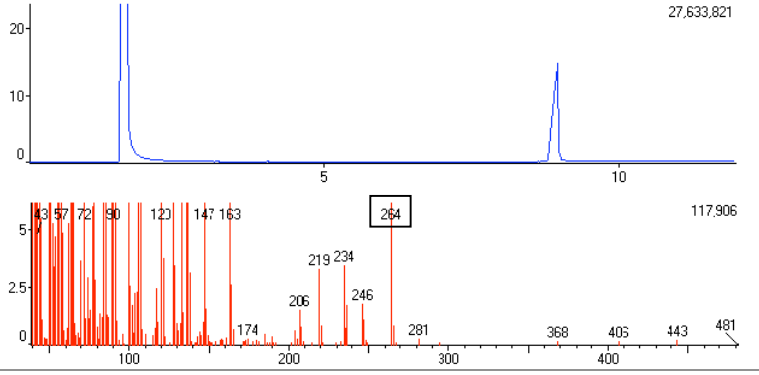

11o[b] 264.2 99%	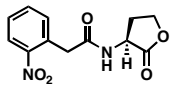	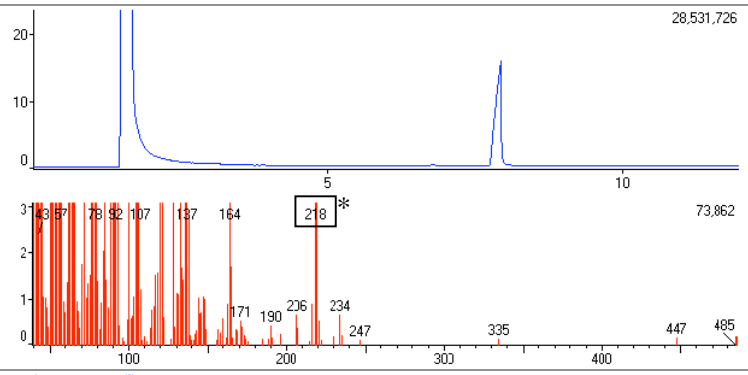
11p[c] 260.3 94.9%	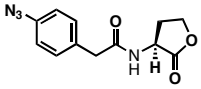	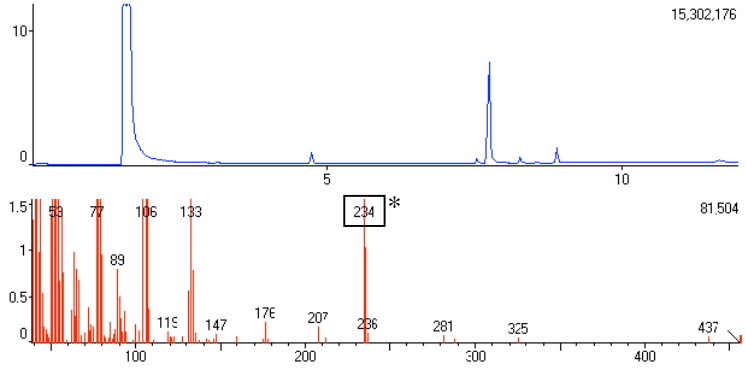
11q 295.3 99%	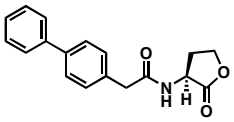	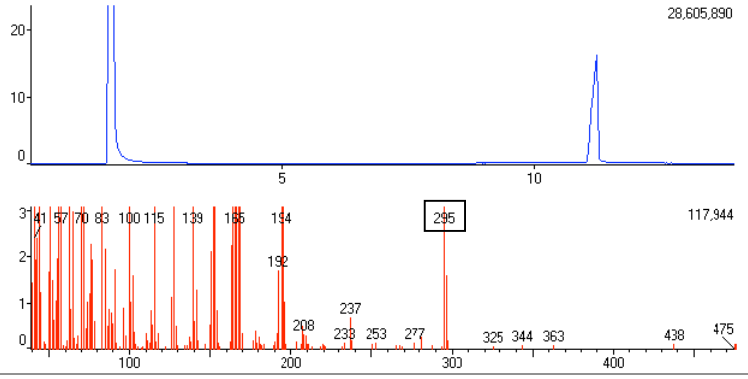
11r 323.4 98.8%	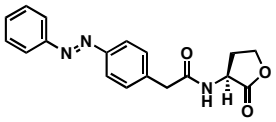	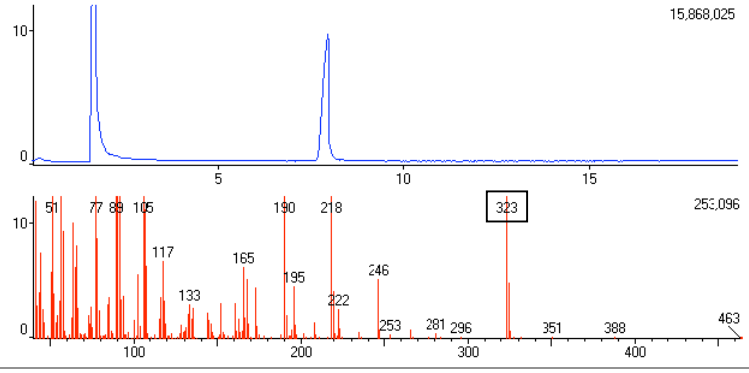

11s 287.2 99%	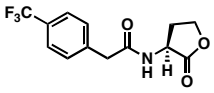	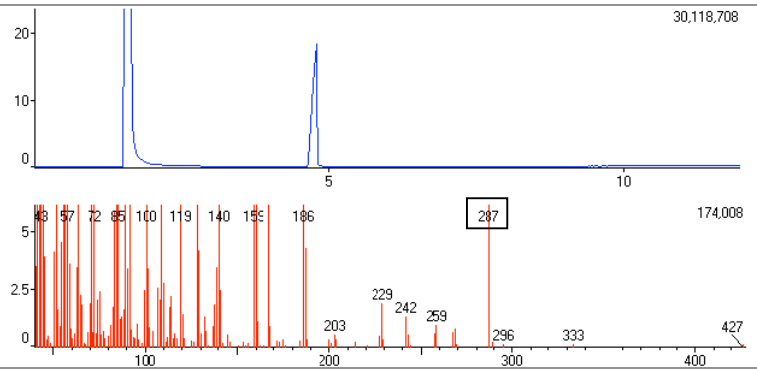
11t 233.3 >99%	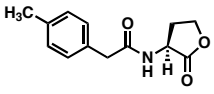	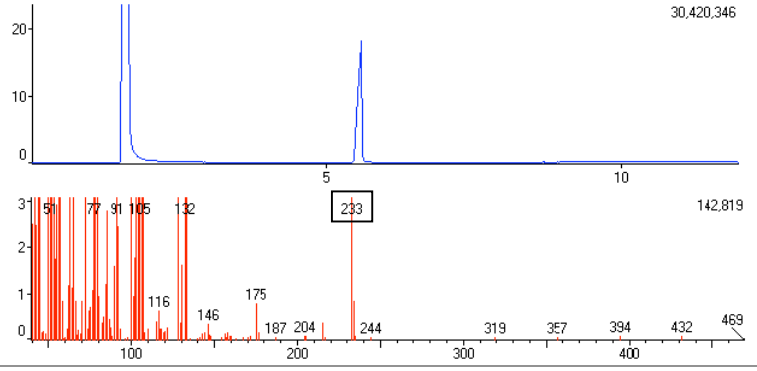
11u[d] 334.4 >95%	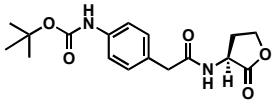	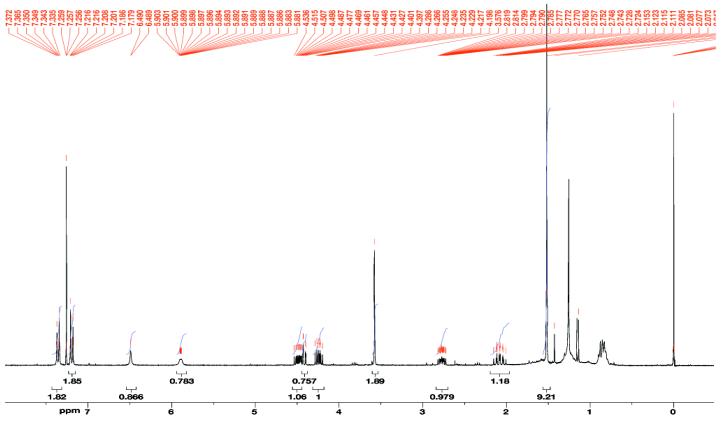
11v 234.3 94.6%	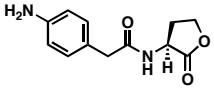	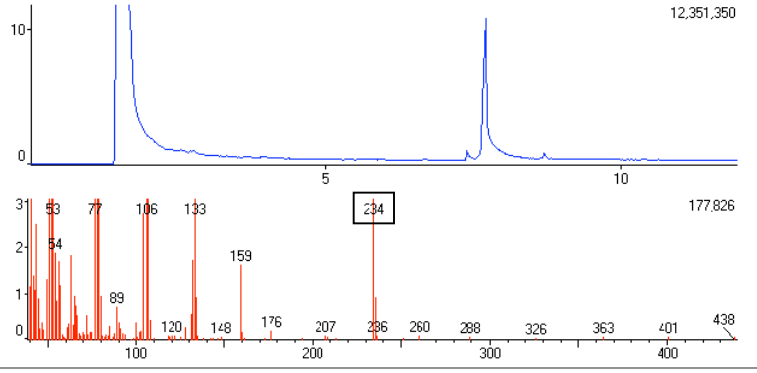

11w 235.3 >99%	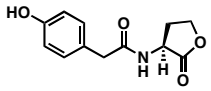	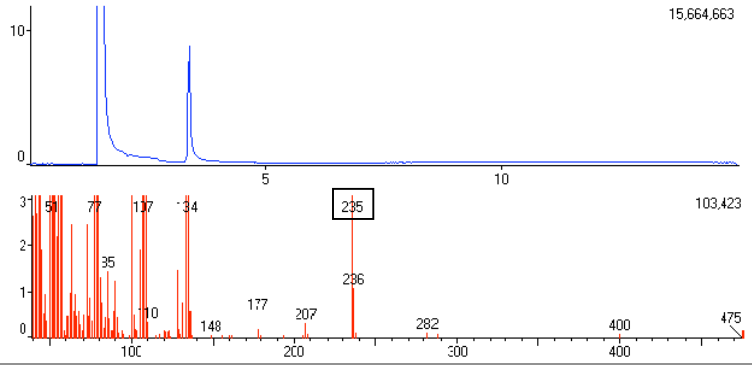
11x 249.3 97.4%	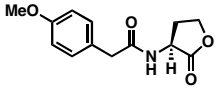	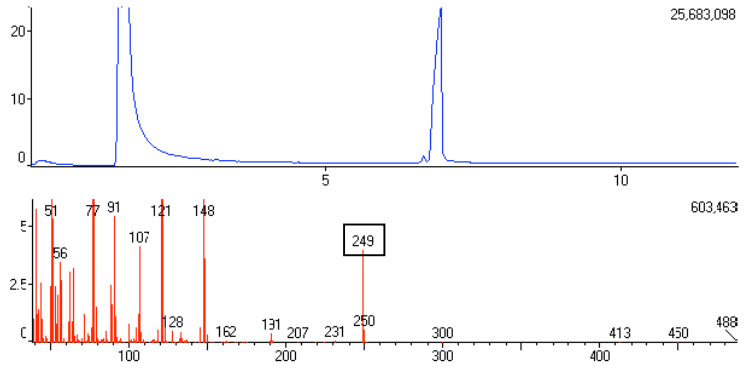

[a] [M-101] equals loss of homoserine lactone.
[b] [M] = 218 equals [M-ortho substituent]. GC spectra indicates a unique compound.
[c] [M] = 234 equals [M-N_2 + $2H^+$]. GC spectra indicates a unique compound.
[d] The Boc group in PHL **11u** was unstable under GC-MS method conditions. The Boc group was present when **11u** was analyzed by ^{1}H NMR ($CDCl_3$, 300 MHz) and ESI.

Biological screening protocols.

Compound handling and reagents. Stock solution of synthetic compounds (10 mM) were prepared in DMSO and stored at -20 °C in sealed vials. The solutions were allowed to come to room temperature prior to use in assays. Solvent resistant polypropylene (Corning Costar cat. no. 3790) or polystyrene (Corning Costar cat. no. 3997) 96-well multititer plates were used when appropriate. All biological reagents were purchased from Fisher and used according to enclosed instructions. LB medium was prepared according to packaging with a pH = 7.5. LBS medium was prepared from 20 g dehydrated LB broth, 15 g NaCl, 30 mL glycerol, and 7.8 g Tris-HCl with a final pH = 7.5.

Instrumentation. Absorbance and luminescence measurements were obtained using a PerkinElmer Wallac 2100 EnVision™ multilabel plate reader using Wallac Manager v1.03 software. A 595 nm filter was used for measuring bacterial cell density (OD_{600}).

***E. coli* assay procedures.** For primary agonism assays, an appropriate amount of concentrated control or PHL (**11**) stock solution, to give a final concentration of 15 μM, was added to wells in a 96-well multititer plate. An overnight culture of *E. coli* JM109 (pSB401)[4]

was diluted 1:10 with LB medium (containing 10 μg/mL tetracycline). A 200-μL portion of the diluted culture was added to each well of the plate. Plates were grown at 30 °C with shaking (200 rpm) until the OD_{600} = 0.35–0.4 (6–8 h). Luminescence then was measured and normalized to cell density per well. Primary antagonism assays were performed in a similar manner except the PHL **11** or control was screened at 15 μM against 20 nM OHHL **1** (EC_{50} of autoinducer in this strain). All assays were performed in triplicate. The primary data is shown below in Figure S-1.

***Vibrio fischeri* assay procedures.** For primary agonism assays, an appropriate amount of concentrated control or PHL (**11**) stock solution, to give a final concentration of 200 μM, was added to wells in a 96-well multititer plate. An overnight culture of *V. fischeri* ES114 (WT, Δ-*luxI* or Δ-*luxR*)[5] was diluted 1:10 with LBS medium. A-200 μL portion of the diluted culture was added to each well of the plate. Plates were grown at RT with shaking (200 rpm) until the OD_{600} = 0.35–0.4 (4–6 h). Luminescence then was measured and normalized to cell density per well. Primary antagonism assays were performed in a similar manner except the PHLs **11** or control was screened at 5 μM against 5 μM OHHL **1** (*ca.* EC_{50} of autoinducer in this strain). Similar methods were used for dose response assays, except the concentrations of controls and PHLs **11** used were between 0.02 and 2×10^5 nM. All assays were performed in triplicate. The primary data is shown below in Figure S-2. IC_{50} and EC_{50} values were calculated using GraphPad Prism software using a sigmoidal curve fit (Figure 2 in main text, Figures S-3–S-5).

The dose response antagonism curves for control AHL **2** and PHL **11m** start to slope upwards at the higher concentrations tested (Figures S-3 and S-4, respectively). Ongoing studies in our laboratory are focused on developing an understanding of this phenomenon.

Primary antagonism and agonism screening data in *E. coli*.

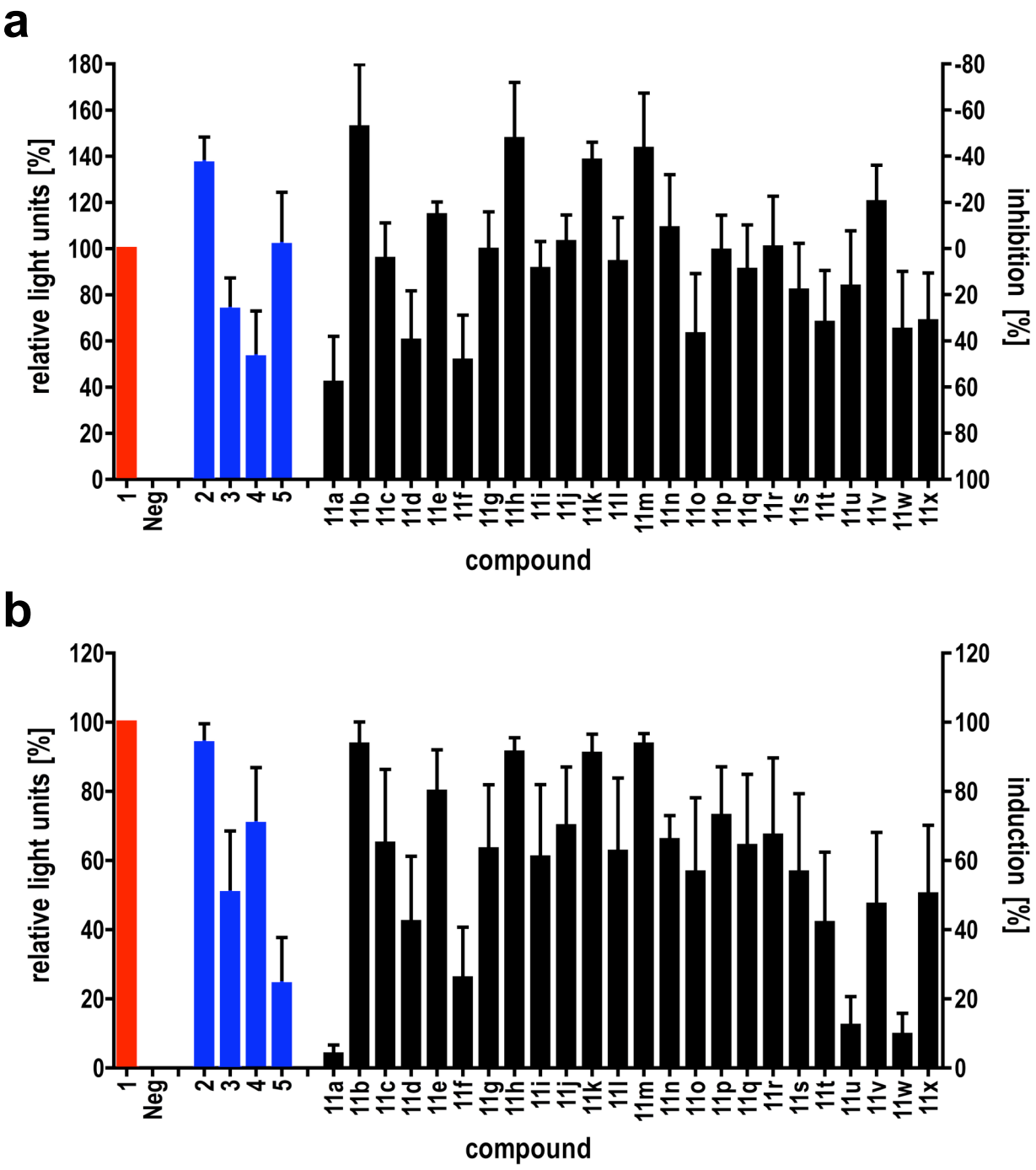

Figure S-1. Primary antagonism and agonism screening data for library **11** in *E. coli* JM109 (pSB401). a) Antagonism screen performed using 15 μM of synthetic ligand against 20 nM of native ligand **1** (red). Negative control (Neg) contains no compound. Control ligands (**2**–**5**) in blue. b) Agonism screen performed using 15 μM of ligand. Error bars, s.d. of the means of triplicate samples.

Primary antagonism and agonism screening data in *V. fischeri*.

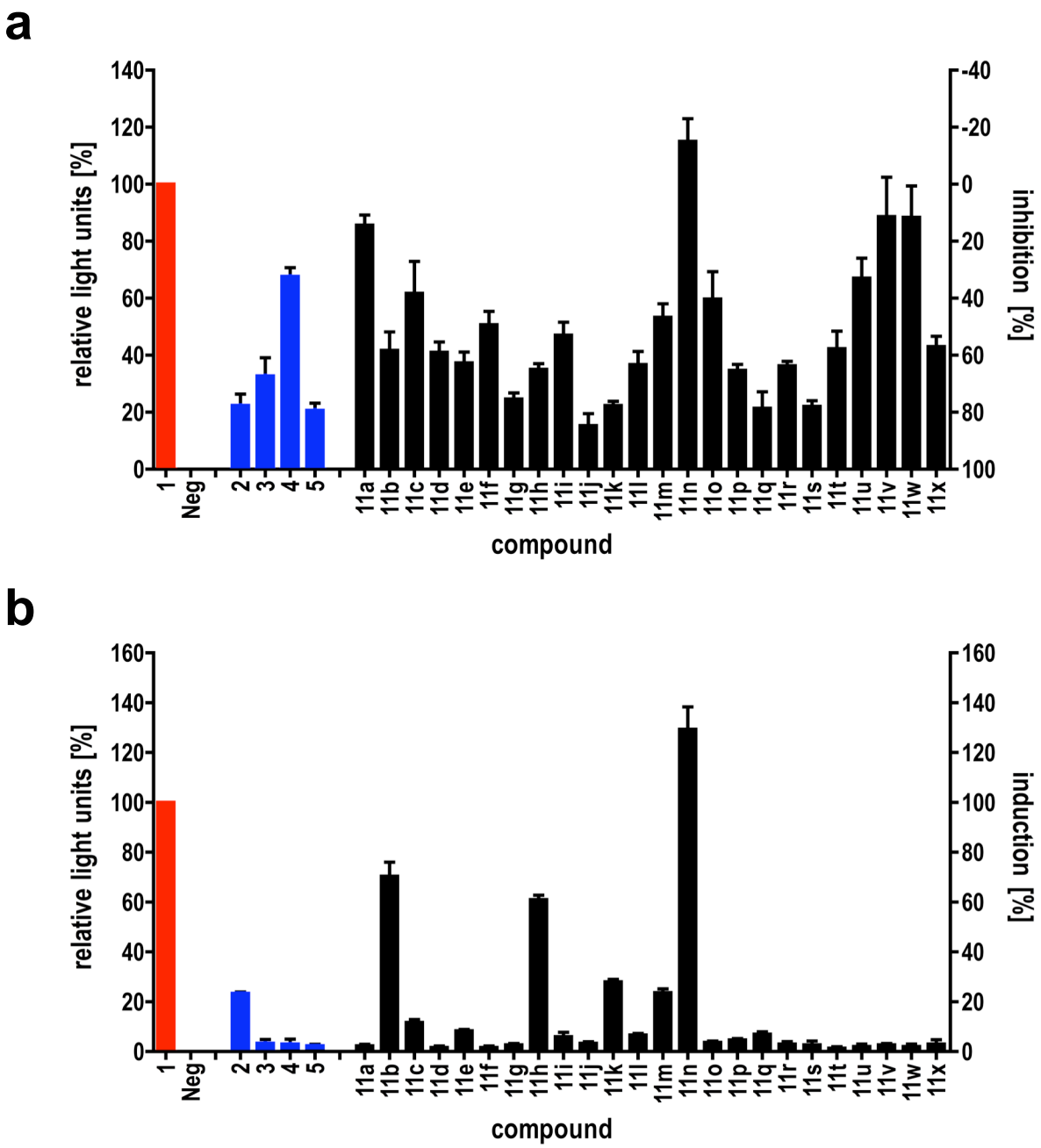

Figure S-2. Primary antagonism and agonism screening data for library **11** in *V. fischeri* ES114 (Δ–*luxI*). a) Antagonism screen performed using 5 μM of synthetic ligand against 5 μM of native ligand (OHHL, **1**). Positive control (**1**) in red. Negative control (Neg) contains no compound. Control ligands (**2**–**5**) in blue. b) Agonism screen performed using 200 μM of ligand. Error bars, s.d. of the means of triplicate samples.

Dose response antagonism data in *V. fischeri.*

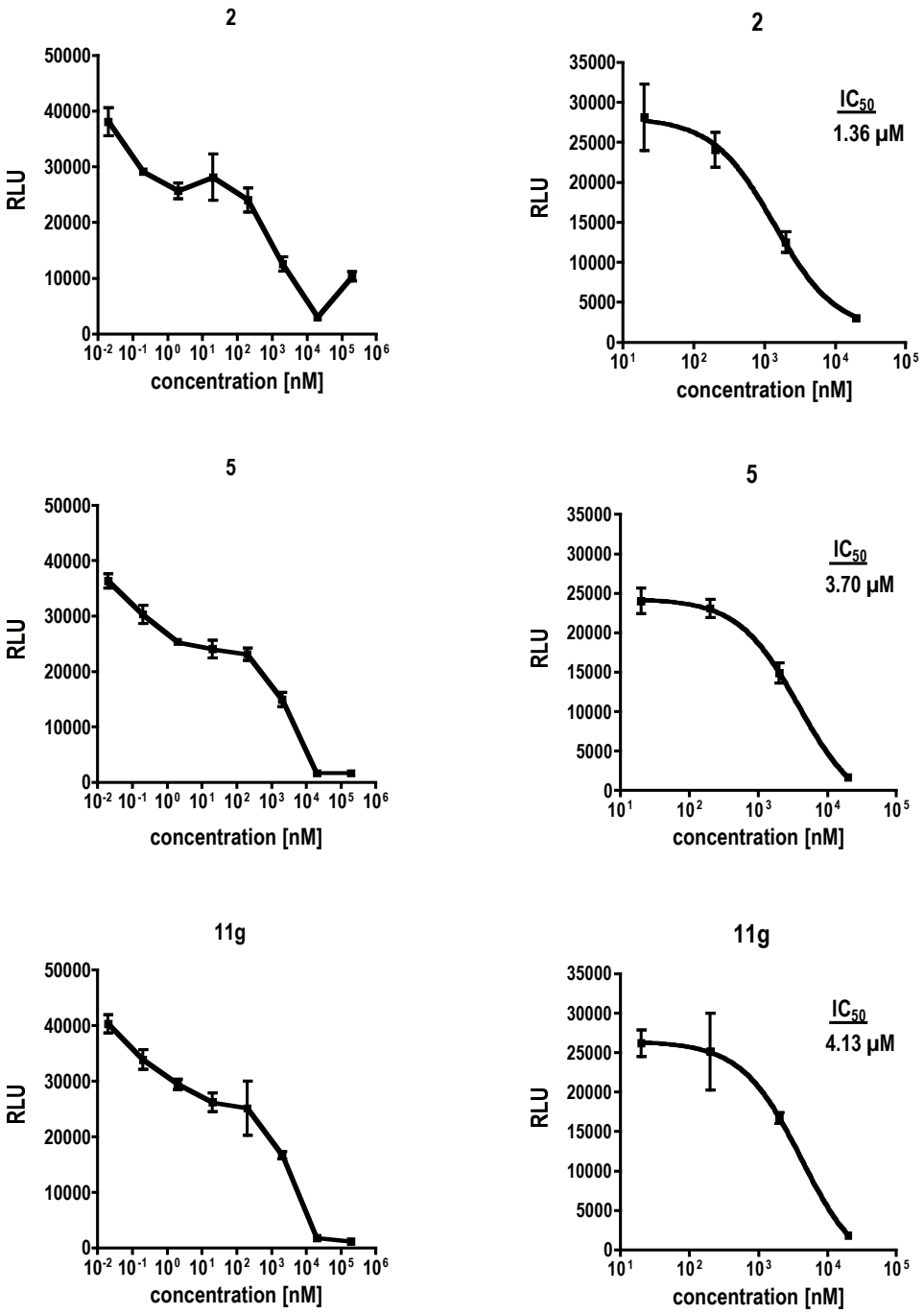

Figure S-3. Antagonism dose responses and IC_{50} values for control compounds **2** and **5** and PHL **11g** in *V. fischeri* ES114 (Δ–*luxI*). *Left:* Full dose response curve. *Right:* Section of dose response curve from which IC_{50} value was calculated. Synthetic ligand screened against 5 μM of OHHL (**1**) over varying concentrations. IC_{50} values calculated using GraphPad Prism. RLU = relative light units. Error bars, s.d. of the means of triplicate samples.

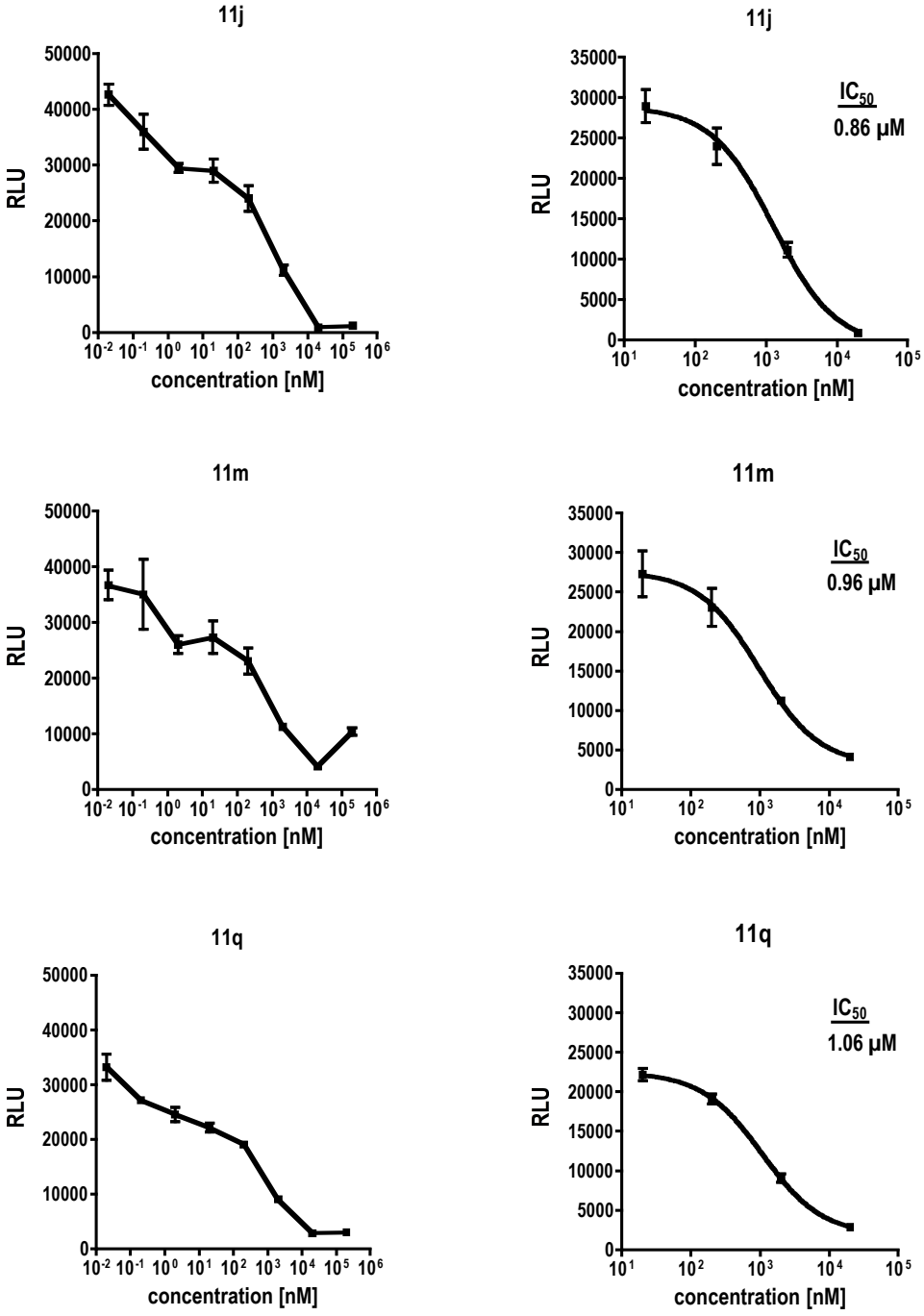

Figure S-4. Antagonism dose responses and IC_{50} values for PHLs **11j**, **11m**, and **11q** in *V. fischeri* ES114 (Δ–*luxI*). *Left:* Full dose response curve. *Right:* Section of dose response curve from which IC_{50} value was calculated. Synthetic ligand screened against 5 μM of OHHL (**1**) over varying concentrations. IC_{50} values calculated using GraphPad Prism. RLU = relative light units. Error bars, s.d. of the means of triplicate samples.

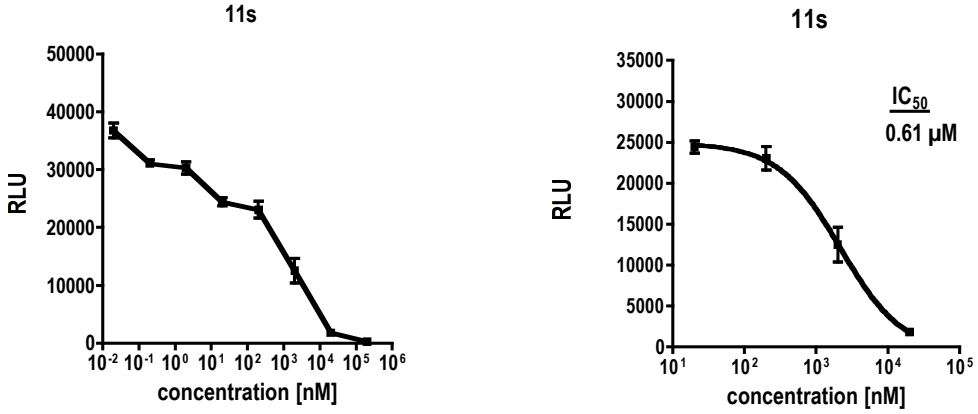

Figure S-5. Antagonism dose response and IC_{50} value for PHL **11s** in *V. fischeri* ES114 (Δ–*luxI*). *Left:* Full dose response curve. *Right:* Section of dose response curve from which IC_{50} value was calculated. Synthetic ligand screened against 5 μM of OHHL (**1**) over varying concentrations. IC_{50} value calculated using GraphPad Prism. RLU = relative light units. Error bars, s.d. of the means of triplicate samples.

Primary antagonism screening data for D-3 and D-5 in *V. fischeri.*

PHLs **D-3** and **D-5** were synthesized according to Figure 1b in the main text except *N*-Fmoc-D-methionine was used instead of *N*-Fmoc-L-methionine (**7**) and were isolated in similar yields and purities as PHLs **3** and **5**, respectively.

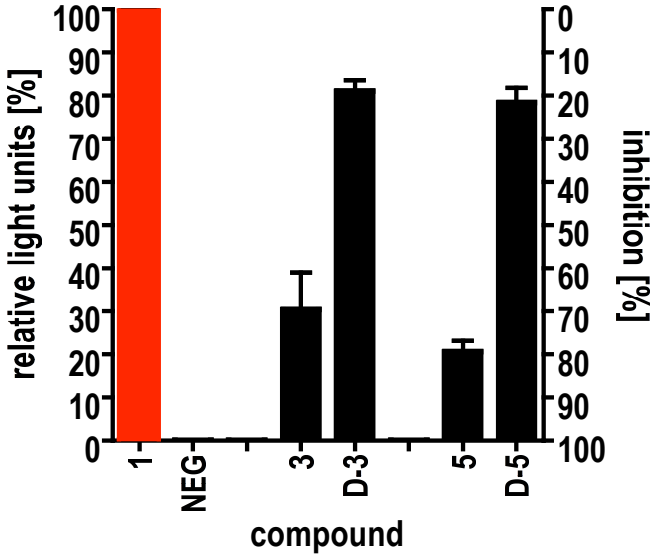

Figure S-6. Primary antagonism data of compounds **3** and **5** and their isomers (**D-3** and **D-5**) in *V. fischeri* ES114 (Δ–*luxI*) at 5 µM of synthetic ligand against 5 μM of native ligand **1** (red). Negative control (Neg) contains no compound. Error bars, s.d. of the means of triplicate samples.

Computational modeling of the *LuxR* ligand binding site and PHL ligands.

Computational methods. All molecular modeling experiments were performed using the MOE software suite (v. 2006.08; Chemical Computing Group of Canada).[6] A model of the AHL binding site in LuxR was generated from the X-ray crystal structure of TraR from *A. tumefaciens* (co-crystallized with its native AHL ligand (*N*-3-oxooctanoyl-L-homoserine lactone; OOHL) and DNA; pdb code:1L3L).[7] This is the only available structure of a LuxR homolog. As there is low overall structural homology between LuxR and TraR (*ca.* 20%), we only performed modeling studies on the binding site region of TraR (*ca.* 80% homology). We defined this site as a sphere with a radius of 12 Å centered on the lactone ring of OOHL. Each of the residues on the TraR ligand-binding site was replaced by the corresponding residues from LuxR according to the sequence alignment by Whitehead *et al.*[8] This alignment has been used in previous homology modeling studies of LuxR.[9]

A conformational database of OHHL (**1**) and selected PHLs (**11**) was created and minimized. The conformations were generated with the MMFF94x force field using Conformation Import in MOE. A limit of 4.5 kcal/mol strain energy was imposed with a 100-conformation limit for each molecule. Duplicate conformations were removed with a heavy atom RMSD tolerance of 0.5 Å (0.75 Å for conformations with strain greater than 3.5 kcal/mol). This database was superimposed over the minimized natural ligand OHHL (**1**) and then scored for best RMS fit. These poses then were docked and minimized into the mutated LuxR binding domain. The docking and minimizations were performed using the AMBER99 force field, with allowance of flexibility of the receptor and gradient change set to 0.01. Ten separate docking poses were determined for each ligand and models were generated from the poses with the lowest overall ligand to receptor strain energy. Selected views of these models are shown below in Figures S-7–S-13.

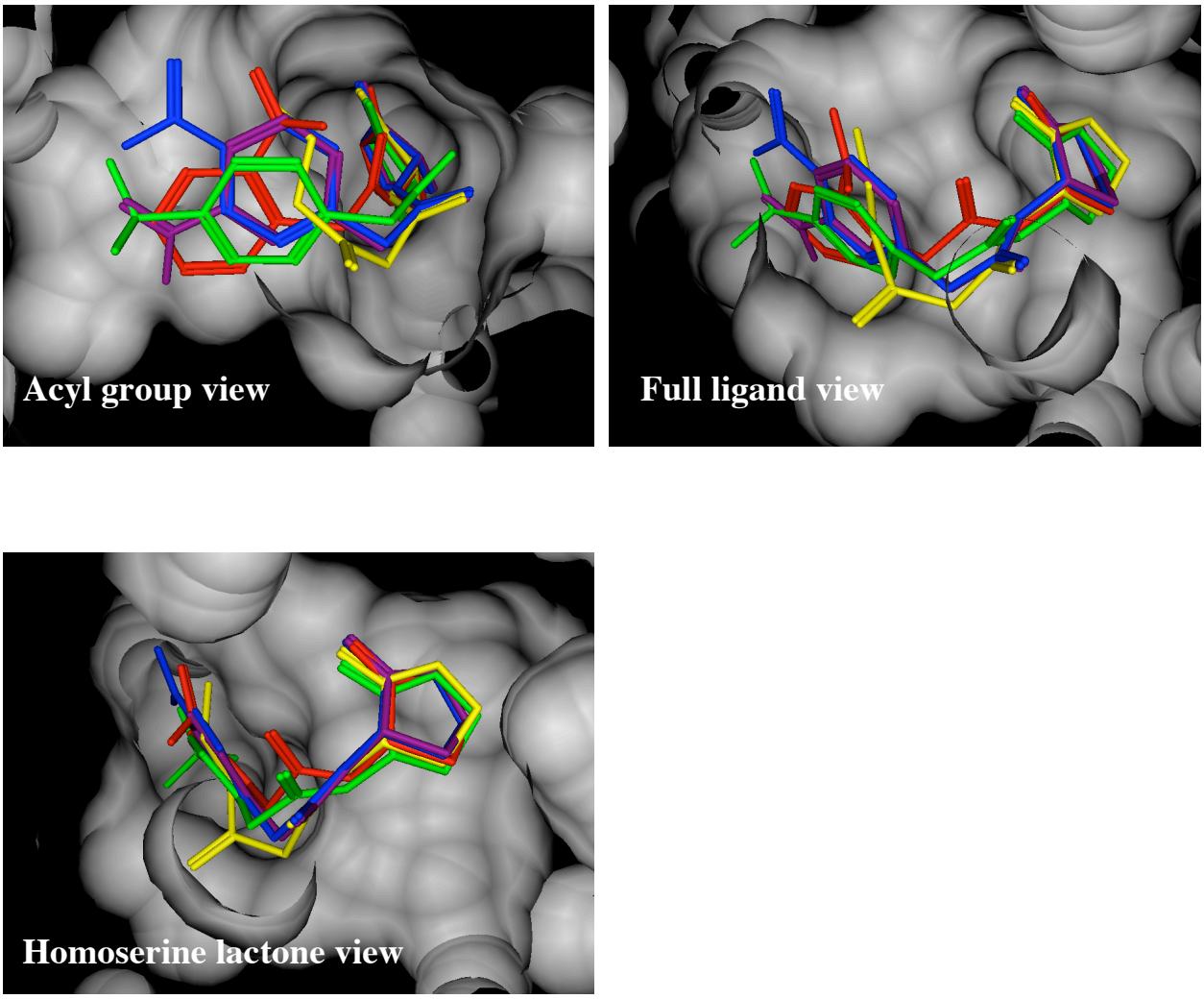

Figure S-7. Three overlaid views of OHHL **1** (yellow) and 4-nitro PHL **11m** (blue), 3-nitro PHL **11n** (purple), 2-nitro **11o** (red) and 4-trifluoromethyl **11s** (green) bound within the modeled LuxR-OHHL ligand-binding site. Surface of LuxR ligand binding domain shown in gray.

a

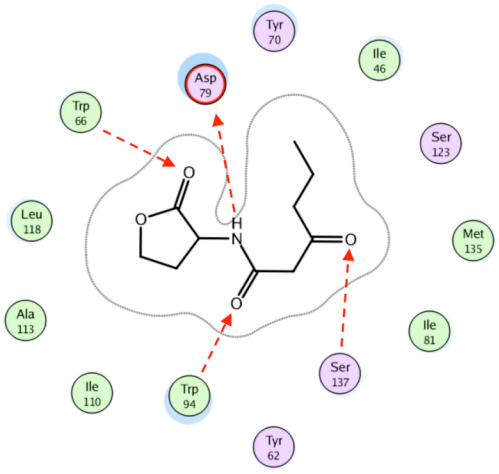

b

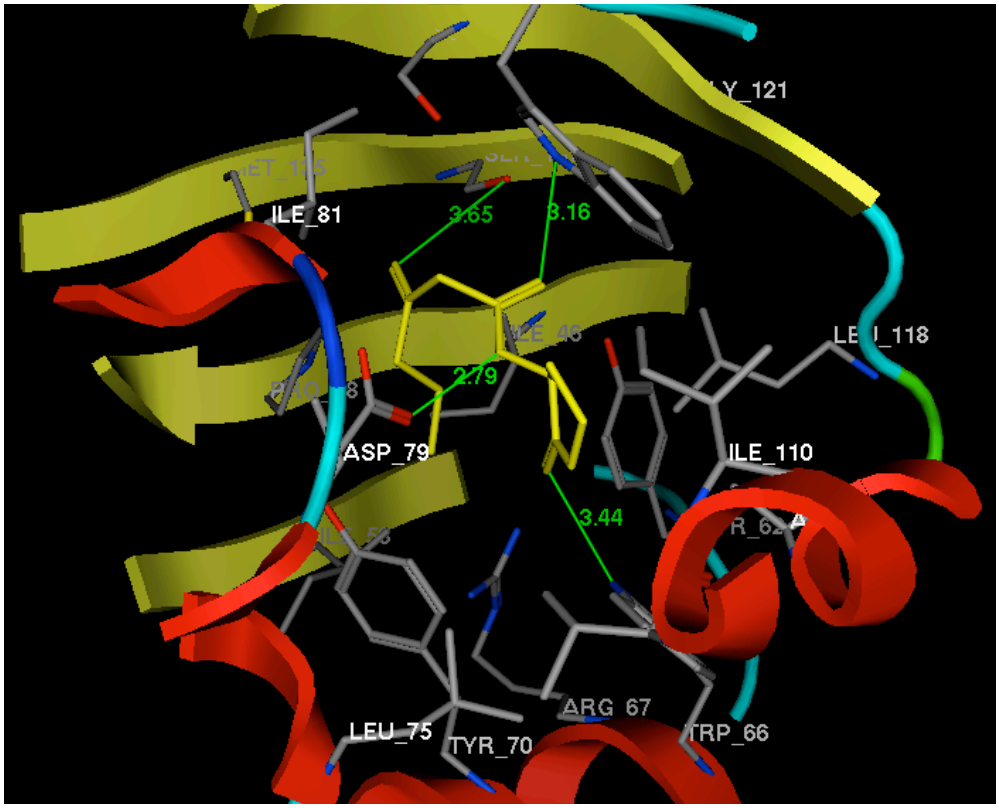

Figure S-8. a) Schematic overview of the possible interactions of the native ligand OHHL (**1**) with the LuxR AHL binding site. Red arrows represent possible hydrogen bonds. A hydrogen bond between Tyr 62 and the amide carbonyl on **1** is also possible; b) Graphical representation of the LuxR binding domain with bound OHHL (**1**). OHHL is shown in yellow. Green lines represent possible hydrogen bonds.

a

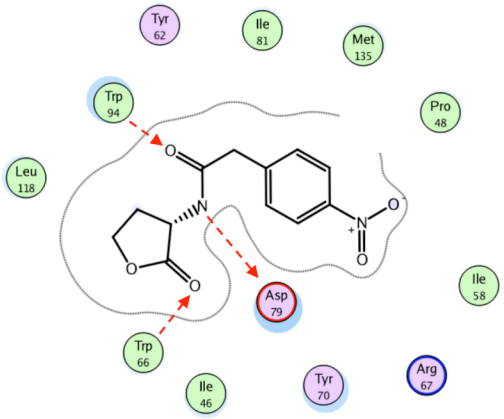

b

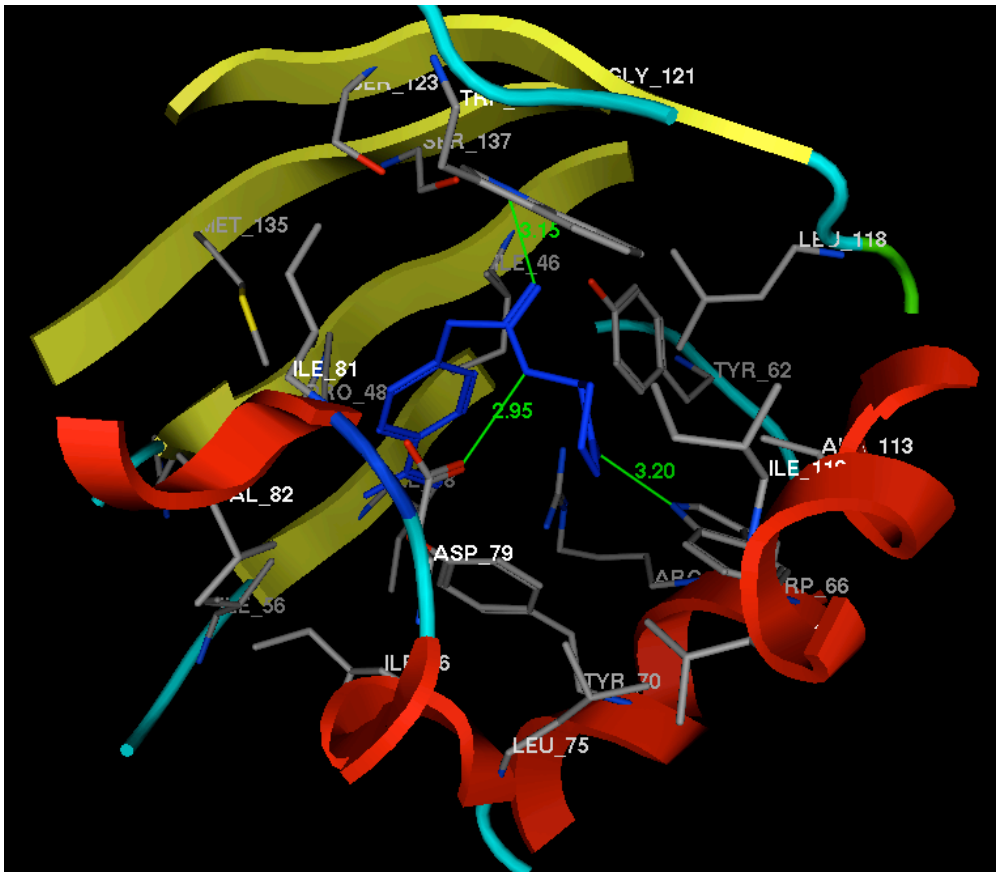

Figure S-9. a) Schematic overview of the possible interactions of 4-nitro PHL **11m** with the LuxR ligand-binding site. Red arrows represent possible hydrogen bonds. A hydrogen bond between Tyr 62 and the amide carbonyl on **11m** is also possible; b) Graphical representation of the LuxR binding domain with bound PHL **11m**. PHL **11m** is shown in blue. Green lines represent possible hydrogen bonds.

a

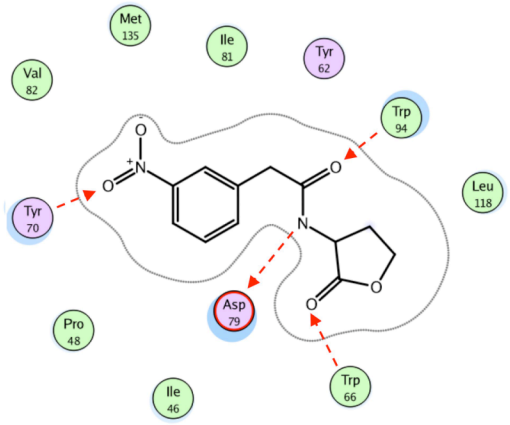

b

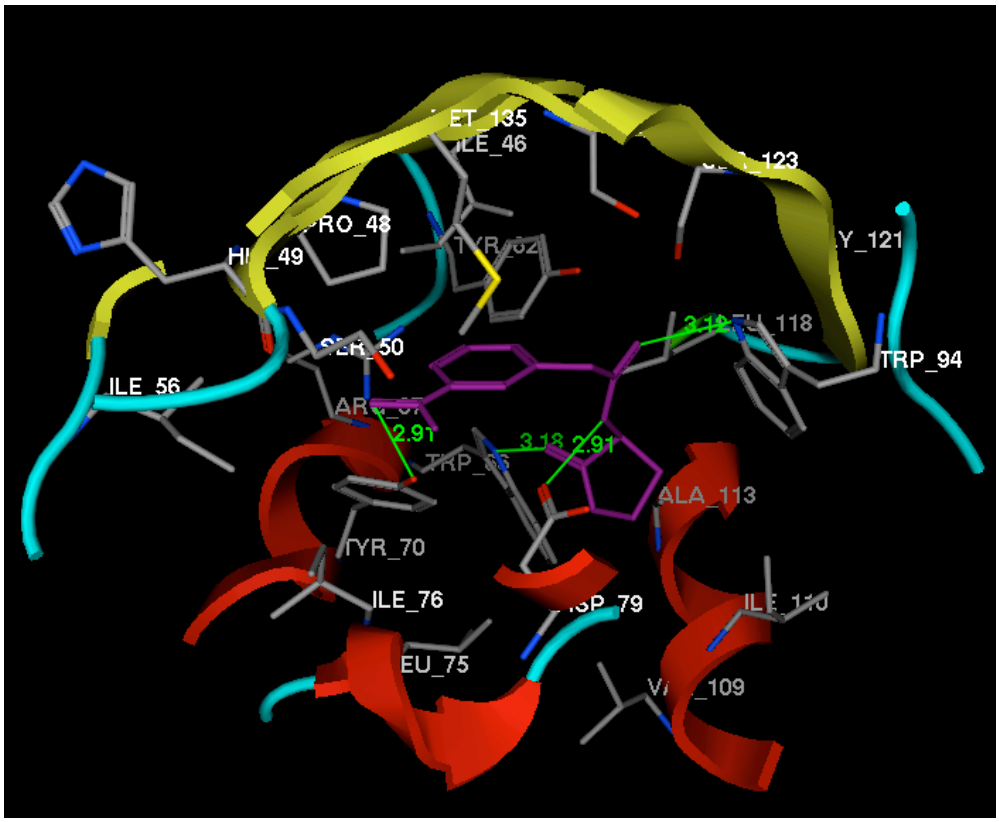

Figure S-10. a) Schematic overview of the possible interactions of 3-nitro PHL **11n** with the LuxR ligand-binding site. Red arrows represent possible hydrogen bonds. A hydrogen bond between Tyr 62 and the amide carbonyl on **11n** is also possible; b) Graphical representation of the LuxR binding domain with bound PHL **11n**. PHL **11n** is shown in purple. Green lines represent possible hydrogen bonds.

a

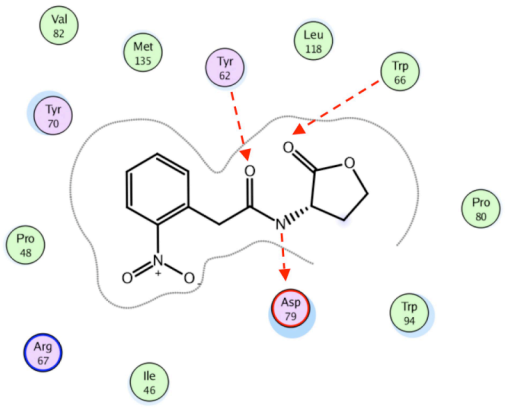

b

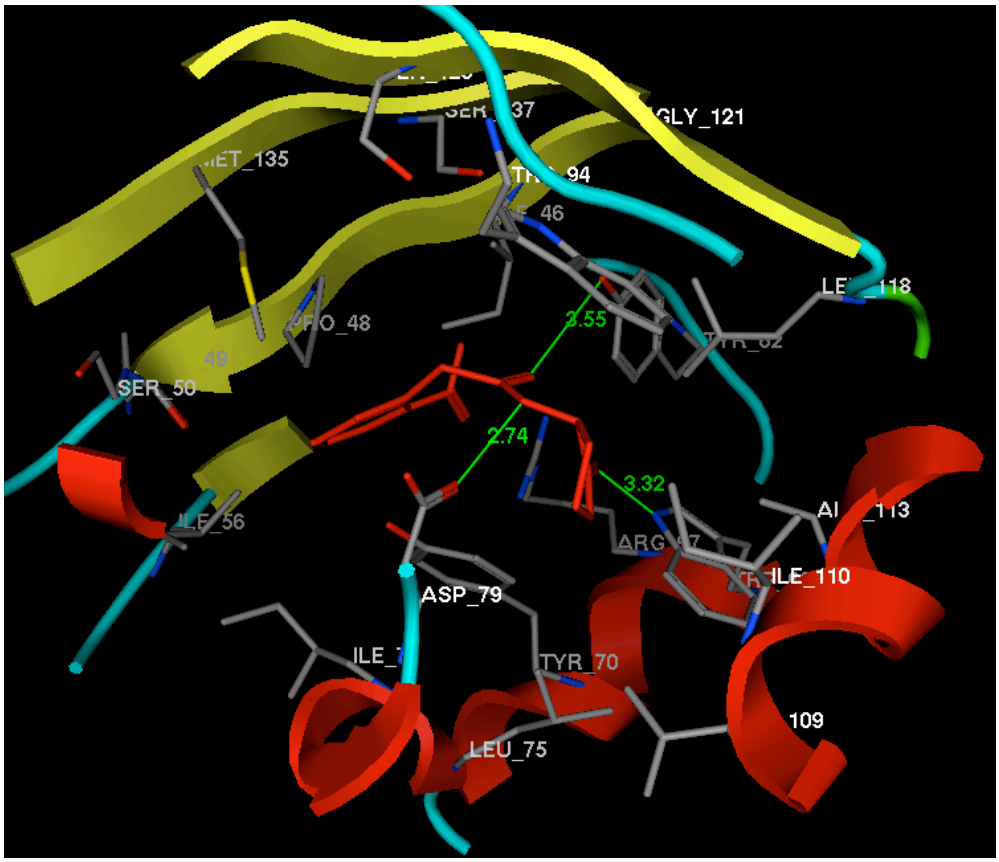

Figure S-11. a) Schematic overview of the possible interactions of 2-nitro PHL **11o** with the LuxR ligand-binding site. Red arrows represent possible hydrogen bonds; b) Graphical representation of the LuxR ligand binding domain with bound PHL **11o**. PHL **11o** is shown in red. Green lines represent possible hydrogen bonds.

a

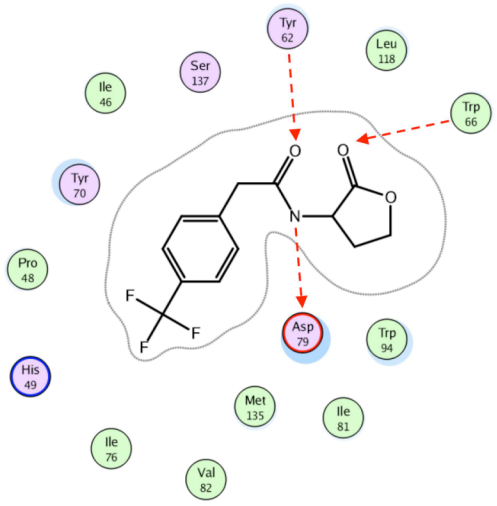

b

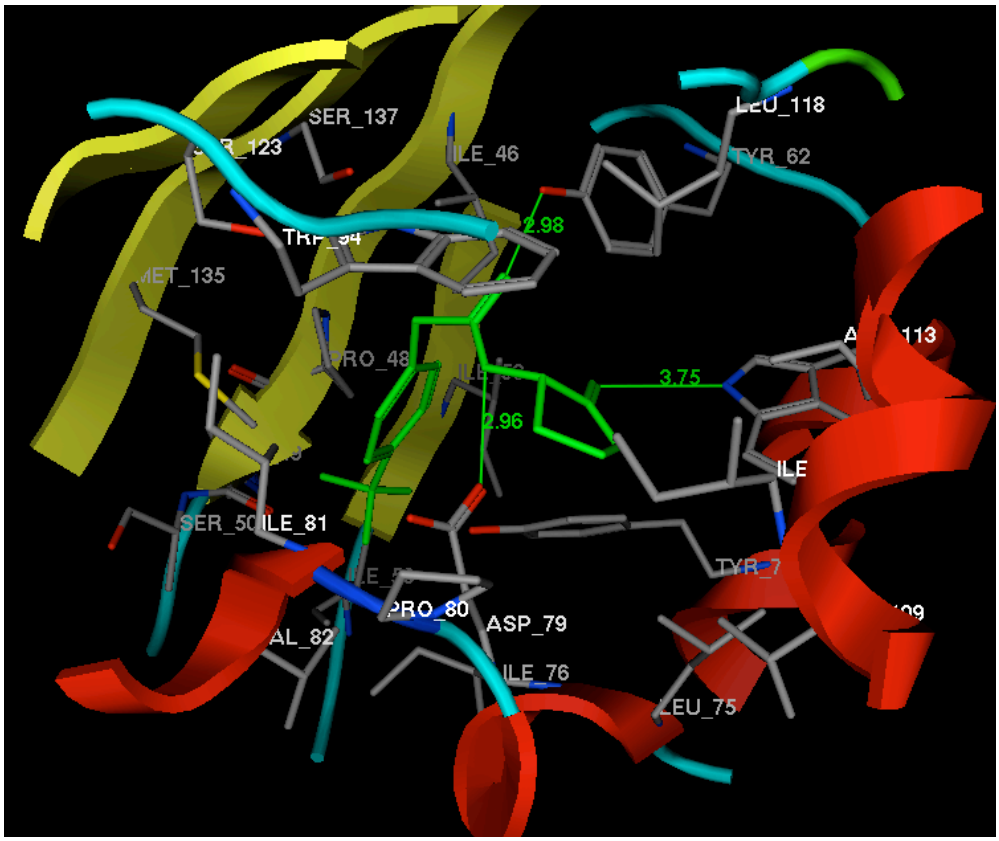

Figure S-12. a) Schematic overview of the possible interactions of 4-trifluoromethyl PHL **11s** with the LuxR ligand-binding site. Red arrows represent possible hydrogen bonds; b) Graphical representation of the LuxR ligand binding domain with bound PHL **11s**. PHL **11s** is shown in green. Green lines represent possible hydrogen bonds.

a

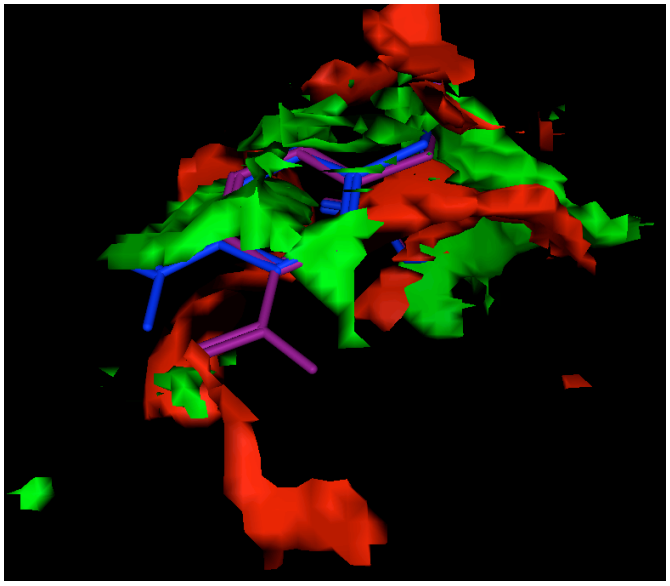

b

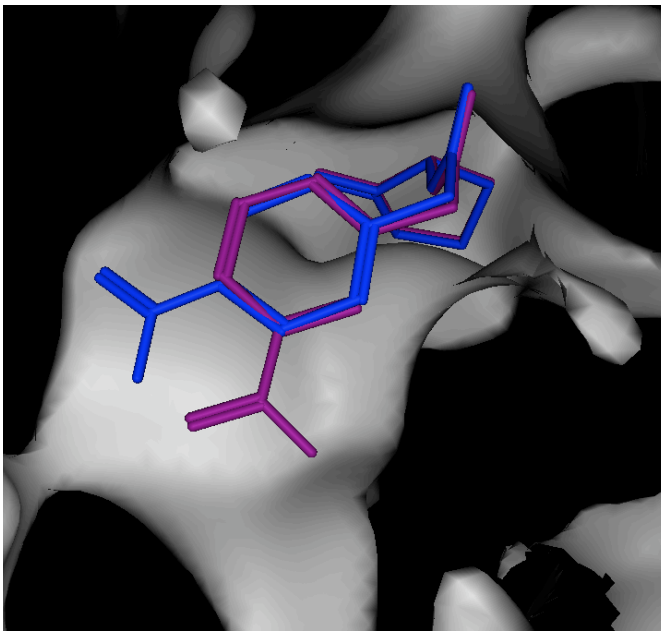

Figure S-13. a) Protein preference contact surface map of modeled LuxR-OHHL binding site with overlaid views of 4-nitro PHL **11m** (blue) and 3-nitro PHL **11n** (purple). Red designates area of hydrogen bond donor or acceptor protein preference and green designates hydrophobic protein preference. b) Overlaid view of acyl chains of PHLs **11m** (blue) and **11n** (purple) bound within the modeled LuxR-OHHL binding site. Surface of LuxR binding site shown in gray.

References and notes.

(1) For more information about the Milestone MW reactor, see: (a) Bowman, M. D.; Jeske, R. C.; Blackwell, H. E. *Org. Lett.* **2004**, *6*, 2019-2022. (b) http://www.milestonesci.com

(2) For more information about the CEM MW reactor, see: http://www.cem.com/

(3) Geske, G. D.; Wezeman, R. J.; Siegel, A. P.; Blackwell, H. E. *J. Am. Chem. Soc.* **2005**, *127*, 12762-12763.

(4) Winson, M. K.; Swift, S.; Fish, L.; Throup, J. P.; Jorgensen, F.; Chhabra, S. R.; Bycroft, B. W.; Williams, P.; Stewart, G. S. *FEMS Microbiol. Lett.* **1998**, *163*, 185-192.

(5) Lupp, C.; Urbanowski, M.; Greenberg, E. P.; Ruby, E. G. *Mol. Microbiol.* **2003**, *50*, 319-331.

(6) For more information on MOE software, including a comprehensive list of publications citing MOE for related homology modeling studies, see: http://www.chemcomp.com/index.htm

(7) Zhang, R. G.; Pappas, T.; Brace, J. L.; Miller, P. C.; Oulmassov, T.; Molyneaux, J. M.; Anderson, J. C.; Bashkin, J. K.; Winans, S. C.; Joachimiak, A. *Nature* **2002**, *417*, 971-974.

(8) Whitehead, N. A.; Barnard, A. M.; Slater, H.; Simpson, N. J.; Salmond, G. P. *FEMS Microbiol. Rev.* **2001**, *25*, 365-404.

(9) (a) Castang, S.; Chantegrel, B.; Deshayes, C.; Dolmazon, R.; Gouet, P.; Haser, R.; Reverchon, S.; Nasser, W.; Hugouvieux-Cotte-Pattat, N.; Doutheau, A. *Bioorg. Med. Chem. Lett.* **2004**, *14*, 5145-5149. (b) Koch, B.; Lijefors, T.; Persson, T.; Nielsen, J.; Kjelleberg, S.; Givskov, M. *Microbiology* **2005**, *151*, 3589-3602.